Home University

Universitat Poliècnica de Catalunya

Barcelona, Spain

Host Institute

Institute of Thermomechanics, CAS

Prague, Czech Republic

Prasad ADHAV Sample Report

Mathematical and Numerical modeling of Rotating Beam using Reduced Order Model (ROM)

Summer Internship

June - August 2018

By
Prasad ADHAV

Guided by

Dr. Chandra Shekhar PRASAD (IT CAS)

Internal Supervisor

Prof. Josep SARRATE (UPC)

Abstract

Rotating beams are useful mathematical models for helicopter rotor blades, wind turbine blades, turbine blades, robotic manipulators and propeller blades. Therefore, the modeling and analysis of rotating beams is an important practical problem. The rotor speed of the blades should be as far as possible from the natural frequencies of the blades so as to avoid resonance and eventually failure. Therefore accurate frequency prediction is important. In initial stages of design it is not required to get the geometry precisely with all its complexities and other parameters associated with it. Therefore, for the free vibration analysis, simple beam elements are used as reduced order models for these complex blades.

The goal is to better understand the already established Euler-Bernoulli and Timoshenko beam theories, which can be used to solve the problem and can be modified to accommodate different variables. One of these variables is rotating speed of the blades. In the practical application discussed here, these "cantilever beams" are rotating with certain speed, the goal is to predict the out of plane natural frequencies, which are affected due to the rotational speed.

The governing equation is to be discretized and a MATLAB code is to be implemented to solve this discretized equation using FEM. The variation of the out of plane natural frequencies is studied for different rotating speeds. Along with natural frequencies, the mode shapes and deformations are studied for various cross-sections of beam. The validation of the model is done using the preexisting validated methods such as Galerkin and Rayliegh-Ritz method.

The study presented in the report is part of the end solution. This structural dynamic analysis is to be later coupled with the fluid system, and the effects of the fluid forces can also be examined on the blades. Thus simplifying the problem and avoiding costly CFD analysis.

Prasad ADHAV Sample Report

Acknowledgements

I would sincerely like to express my gratitude to all those who supported and helped me during my internship.

First and foremost, I would like to thank my primary advisor Dr. Chandra Shekhar PRASAD for his constant guidance and encouragement. Without him, the work carried out during the internship would not be possible. I also thank him for inspiring with all the knowledge he shared. I would like to thank Patrick Zima for bringing my application to light and availing this amazing opportunity.

I would like to thank my parents Rajkumari and Suresh ADHAV, for their unconditional love and support.

I would like to thank Lelia ZEILONKA for her unrelenting support throughout the duration I have known her.

I would like like extend my gratitude to my friends Tejas NATU, Pradeep BAL and Luan MALISKOWSKI for their help and support in my work. And lastly I would like to thank Rohit KUWAD for making my stay in Prague memorable.

Prasad ADHAV Sample Report

List of Symbols

A	cross-sectional area of rotating beam
E	Young's modulus
f	non-dimensional natural frequency
f_z	Vertical load per unit length
f_H	axial force parallel to horizontal axis
H_i	Hermite's shape functions $i = 1, 2, ...4$
Ix	moment of inertia about x-axis
I	moment of inertia about principle axis
J	kinetic energy
K_{ij}	ij^{th} element of stiffness matrix
K	global stiffness matrix
K_n	elemental stiffness matrix(n = element no.)
L	length of rotating beam
l	length of element
m	mass per unit length
m	mass-matrix
m_{ij}	ij^{th} element of mass matrix
M	bending moment
r	radius of beam from rotational axis
S	shear force
t	time
T	axial force
U	total strain energy
U_f	strain energy due to flexure
U_s	strain energy due to shear
V_x	velocity along x-axis
V_y	velocity along y-axis
V_z	velocity along z-axis
w	Vertical deflection of beam
w_{app}	approximated Galerkin function
x	x-axis and distances along x-axis
z	z-axis
ϵ	error
ε	strain
λ_i	i^{ht} eigen value
ω_i	i^{ht} natural frequency of rotating beam
Ω	rotating speed of beam
ϕ_i	i^{ht} mode shape function
ρ	density of the beam material
θ	deflection slope
$\dot{(\ )}$	first order differentiation of a variable with respect to time
$\ddot{(\ )}$	second order differentiation of a variable with respect to time
$(\ )'$	first order differentiation with respect to horizontal axis
$(\ )''$	second order differentiation with respect to horizontal axis

Prasad ADHAV Sample Report

Contents

Prasad ADHAV Sample Report

1 Introduction

1.1 Background

Early studies on rotating beams appear in the 1920s, from the turbo-machinery industry. Many studies have treated the problem with linear models like Jones 1975. Initially their was the classical Euler-Bernoulli Beam theory which can be applied for slender beam problems and then Timoshenko 1940 proposed the beam theory which can be applied for thick beams, it accounted for shear effects, which is now known as the Timoshenko beam theory. One can find a plethora of literature based on beam theories for static beams. A good foundation of basics in theories of beam using FEM can be found in Onate 2013. But literature concerning rotating cantilever beams is less and it is very recent. Even now there is active research being done in this field to solve the problem and issues related to it. Similarly Ganguli 2017 gives a good foundation in the field of FEM for rotating beams, but these books are very recent.

From the literature it is observed that the matrices needed for FEM of beams were developed in the $1960's$, for example Luke 1969. Later on, based of these developments, in the $70's$ it is seen that the free vibration analysis of beams started, where natural frequencies of the beam are computed with as minimum error as possible, simultaneously working on computational aspects of various methods Luke 1969; Goodwin 1966; W. E. Boyce and G. H. Handelman 1961; Jones 1975.
The problem of determining the influence of a tip mass on natural frequency of transverse vibration of a uniform beam clamped at one end, was first studied in connection with the design of helicopter blades by G. Handelman, W. Boyce, and Cohen 1958. But it wasn't until the $80's$ where the practical application potential of rotating beams was truly realized, such as turbine and wind turbine blades, air plane propellers, in recent years robotic arms, satellite booms etc, apart from helicopter blades.

In the recent years we can see more and more work related to developing new elements, modifying and improving old methods, implementations in non-linear geometries, composite beams etc, thus taking the scope for practical application of beams further. Also now methods and models can be seen where we can incorporate the coupling effects of shearing, Coriolis acceleration, in-plane vibrations, out of plane vibrations and centrifugal stiffening with greater accuracy. Most recent study by Yang et al. 2018 have presented their results of the gyroscopic and centrifugal stiffening effect as a coupled system in their paper. Due to this coupling, the eigen value problem becomes very complex to solve.

Similarly, due to the technology and resources available, research and development of various real life systems is becoming more and more complex very rapidly. Not only are they becoming complex, but they are getting huge. We now need more and more computational resources such as supercomputers, costly commercial softwares and very skilled manpower to perform these simulations. This possesses two huge problems, cost in terms of money as well as computational cost and time. Many people, research labs and even corporate companies cannot afford both. Current market for accurate, fast and cheap computational tools is growing. So reduced order modeling is a very highly likely candidate to become a commercial solution for such needs. Many a times in design phase we do not need each and every little parameter value accurately. We just need a few main, highly influential parameters with an acceptable accuracy. ROM takes advantages of redundancies in space or time or other parameters, and identifies "genuine" degrees of freedom and gives low dimensional approximation while preserving a satisfactory accuracy and effectively reducing computational resources needed. This is what exactly is needed and in demand. The above mentioned needs are clearly demonstrated in the comparison be between CFD and Volterra based ROM by Lucia, Beran, and Silva 2004, where full CFD solution, consisting of 8000 iterations required approximately 24 hours on an SGI Origin 2000 computer with 4 CPUs. By comparison, the Volterra based ROM response required about a minute.

ROM allows systematic generation of cost effective representations of large scale systems or com-

Project ADMV Sample Report

plex systems resulting from discretization of PDE's. ROM has various applications in the fields of fluids, Fluid-Structure interaction, Structural dynamics, circuit design, piezoelectric and other interdisciplinary problems. In the last decade a lot of different methods have been proposed for ROM, which can be seen in Shabana 2013; Schilders, Van der Vorst, and Rommes 2008; Diest 2013; Bui-Thanh, Willcox, and Ghattas 2008.

The simple cantilever beams are used as reduced order model for complex turbine blades. In the literature survey presented, the objective is to understand the implementation of ROM using the various beams theories, for dynamic analysis of cantilever beams. It is of much interest to know the natural frequency of stationary as well as rotating beams, as the focus is to know the deformations and mode shapes due to the vibrations caused, and its effects on the beam.

Although this all sounds very tempting, but after further study of literature, it can be observed that there are still a number of open issues, including the reliability of reduction techniques, guarantees associated with the quality of reduced model and validity of model over a range of operating conditions. But considering the growing trend it is expected that these shortcomings will be resolved in coming years.

1.2 State of Art

From Hodges and Rutkowski 1981, one can finally find some reliable results obtained from FEM. They used variable order FEM, and also presented some corrected results for Hao in their paper and compared those results to their own for first five modes for uniform as well as tapered beam. In their paper they derived the finite element equations by applying the principle of virtual work and applied the Galerkin formulation in FEM. Now that the natural frequencies of rotating beams can be calculated fairly accurately, and closer to the exact solution through free vibration analysis, in later works such as Wright et al. 1982, it is seen that the study of effects of centrifugal stiffening. In his paper he illustrated the decreasing influence of centrifugal stiffening effect with increasing mode numbers. And this opened a lot of opportunities for further study and solving problems involving vibrations of propellers, helicopter blades and turbine blades etc. Yokoyama 1988 then published his work based on the Timoshenko beam theory, which incorporated the shear effect in the beam deformation. Until Yokoyama, many studies had focused only on out-of-plane vibrations and had neglected the effects due to shear deformation and rotary inertia.

He used Hamilton's principle for deriving the governing equation. The finite element method presented in his paper assumed cubic distribution of displacement over the beam element and used 8 shape functions. With his method using 8 elements, the results obtained were found to be very close to the "exact" solution achieved by Hodges and Rutkowski 1981 with one element and 15^{th} order displacement function. Owing to the stiffening effect of centrifugal force considered the in plane natural frequencies were found to increase with increase in rotational speed. Although results obtained were reliable, it should be kept in mind that still, a reliable study of coupling effect of shearing deformation and rotary inertia wasn't present. It should be also noted that only linear geometries were considered in the studies mentioned, but in the $80's$ and $90's$ studies on geometrically non-linear beams had been started, varying from simple prismatic beams till advanced curved beam geometries Ibrahimbegović 1995. Also, a lot of studies were made and non-linear strains, shape functions were proposed Sharf 1999 so as to accommodate the coupling effect. In these papers, results were presented which confirmed the centrifugal stiffening effect which is responsible for increasing the natural frequency and simultaneously decrease in the shear effect, with the increase in rotational speed Banerjee 2001.
Banerjee 2001 presented formulation and free vibration analysis of centrifugally stiffened Timoshenko beams by extending the dynamic stiffness method he published in 1999. He used Hamilton's principle

Prasad ADHAV Sample Report

to derive the governing differential equation. He included the effect of an arbitrary hub radius. Using Frobenius method of series solution and imposing the boundary conditions, he formulated the dynamic stiffness matrix which is related to amplitudes of harmonically varying forces with harmonically varying displacements.

Typically a conventional finite element method(CFEM) for rotating beam uses cubic polynomials as interpolating functions and usually convergence to some extent is achieved by increasing number of elements. In Ganguli 2017,it is explained that to illustrate a method's effectiveness in dynamic analysis, it is a good practise to evaluate at least first 5 modes, because if an impulsive force is applied at the tip, almost all modes get excited, but most response contribution comes from first three to four modes.For capturing these modes can need many elements which leads to a large size eigen value problem, thus resulting in large degree of freedom(DoF). FEM analysis. Hence, there was a need for simpler, low DoF method. To address these shortcomings of CFEM Wang and Wereley 2004 proposed a spectral Finite element method(SFEM) for low DoF, dynamic analysis of rotating tapered beams. In their paper the goal was to get a reduced order DoF compared to CFEM but also maintain high accuracy of mode frequency, mode shape and force response predictions, all the while using even as fewer elements as possible. There model was based on the exact solution obtained from Frobenius power series same as Wright et al. 1982. Wang and Wereley validated the method by the exact solutions and results obtained by Wright et al. 1982 and Hodges and Rutkowski 1981. Though they used only one tapered element instead of several uniform elements, they used a large number of terms from Frobenius power series.

Also, SFEM uses solution obtained in frequency domain, the natural frequencies are obtained by solving transcendental equations instead of solving eigen value problems like in CFEM, which can be complicated. It is always advantageous to use less number of elements, by using accurate finite element models for obvious reasons. Hence Gunda, Singh, et al. 2007 proposed a superelement using a combination of polynomials and Fourier series as a shape functions. The superelement gives comparable results with the use of only one superelement with 14 DoF compared to the 50 elements of CFEM with cubic shape functions and a total of 100 DoF for the rotating cantilever beam. In Gunda and Ganguli 2008, they also proposed a new rational interpolation functions for FEM analysis of rotating beams which were obtained by satisfying the PDE of Euler-Bernoulli beam theory. The shape functions turned out to be dependent on rotational speed and element position along the beam and they accounted for the centrifugal stiffening effect . This was an issue with the CFEM and Hermite's cubic shape function presented in Ganguli 2017

Considering the huge scope of practical applications, the research and development in the field have increased drastically over the last decade. Huang, Lin, and Hsiao 2010 in their work present a method based on power series solution to solve natural frequency of very slender beam at higher angular velocity. They also presented the coupled effect of Coriolis force, angular velocity and slenderness ration on the natural frequency of the rotating beam.

Rafiee, Nitzsche, and Labrosse 2017 in their paper give a review of the development in the field of dynamic analysis of beams of the recent years, they compared various methods, stated their advantages and disadvantages, and future prospects. Considering, the need for research and development in dynamic analysis started so as to replace complex systems with simpler one's, but those simple systems also have become a bit complex considering computational and time costs. Hence, a lot of people have diverted their attention towards Reduced Order Modeling(ROM). ROM is discussed in the next section.

Prasad ADHAV Sample Report

1.3 Discussion

Rotating beams are useful mathematical models for helicopter rotor blades, wind turbine blades, turbine blades, robotic manipulators and propeller blades. Therefore, the modeling and analysis of rotating beams is an important practical problem. In the following sections, approximate method is employed for obtaining frequencies of rotating beams. A good reduced model of a rotor blade is an elastic cantilever beam. The governing equation is obtained from the classical beam theory.

Prasad ADHAV Sample Report

2 Mathematical Model Formulation

Euler-Bernoulli beam theory is the simplest beam theory available. It is applicable to the slender beams. The assumption in this beam theory is a plane section normal to the neutral axis (beam axis) remains plane after deformation. It is also assumed that shear deflection is negligible and rotary inertia is neglected. This implies that the effect of rotation of element is small compared to vertical displacement. But the Timoshenko beam theory accounts for the effect of shear deformation. Therefore, Timoshenko beams are more suitable for thick beams ($\lambda = \frac{L}{h} < 10$), but it is also applicable for slender beams ($\lambda > 100$), though the shear effect is irrelevant for the slender beams. In the formulation it is planned to use the 2 noded beam element. The weak form of the governing equation is to be achieved. And this weak form the is to be discretized according to the Finite elements method. After discretization of the weak form, the multiple element system can be represented in form of matrices. These matrices are nothing but the eigen value problem, upon solving which, the natural frequencies and mode shapes are to be obtained. The main focus will be to find the natural frequencies of the 4 digit NACA profile, since it is the cross section which is closest to the real geometry of the rotor blade.

2.1 Mathematical model development

While developing the mathematical model, there are some basic assumptions considered so as to make it easier task to get the governing equation. A beam of length L and cross-sectional area A is considered on the plane xz which is assumed to be principle plane of inertia. It is also assumed that the beam axis coincides with the x-axis. The material properties are assumed to be isotropic and homogeneous, so that beam axis coincides with the neutral axis. In addition, structural damping is neglected. The beam theory is based on the following hypotheses:
1. The vertical displacement (deflection) w of the points contained on a cross-section are small and equal to the deflection of the beam axis.
2. The lateral displacement is zero.
3. Cross sections normal to the beam axis before deformation remain plane but not necessarily orthogonal to the beam axis after deformation.

The following mathematical model for rotating beam is developed in the book Finite Element Analysis of Rotating Beams by Ganguli 2017.

Consider a blade section as shown in figure 2.2. Here, $f_z(r,t)$ is vertical load per unit length and $w(r,t)$ is vertical deflection at a distance r. The forces acting on this blade are: $m\ddot{w}dr$ is the inertia force, $f_z dr$ is the external force, $f_H dr$ is axial force parallel to r, T is the axial force (positive for tension), S is the shear force at the cross-section, M is the bending moment.

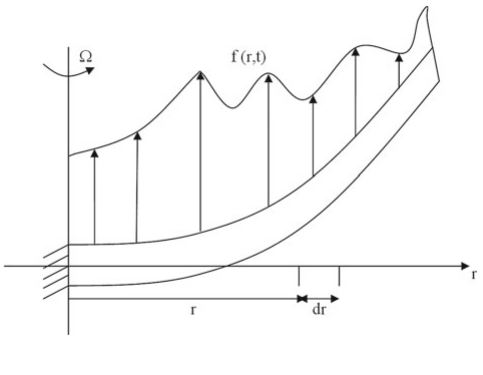

Fig 2.1 Elastic blade

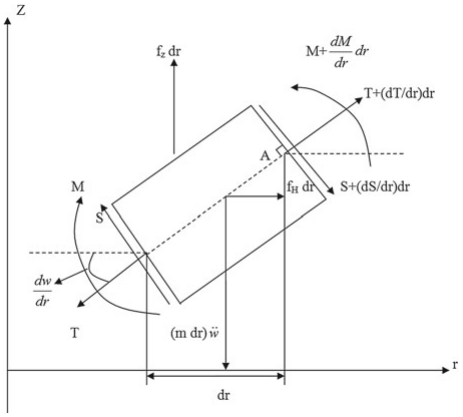

Fig 2.2 Elastic blade section

$\frac{dw}{dr} = \theta$ is the deflection slope, assumed to be small. Therefore,

P... ADHAV Sample Report

$$cos\left(\frac{dw}{dr}\right) \approx 1 \qquad sin\left(\frac{dw}{dr}\right) = \frac{dw}{dr} \tag{2.1}$$

Equilibrium of forces on the element, in r-direction yields

$$\sum F_r = -T + T + \frac{dT}{dr}dr + f_H dr - S\frac{dw}{dr} + \left(S + \frac{dS}{dr}dr\right)\left(\frac{dw}{dr} + \frac{d^2w}{dr^2}dr\right) = 0 \tag{2.2}$$

Forces in z-direction yield,

$$\sum F_z = f_z dr + S - S - \frac{dS}{dr}dr - m\ddot{w}dr - T\frac{dw}{dr} + \left(T + \frac{dT}{dr}\right)\left(\frac{dw}{dr} + \frac{d^2w}{dr^2}\right) = 0 \tag{2.3}$$

Now, the moment about point A in figure 2.2

$$\sum M = M + Sdr - M - \frac{dM}{dr}dr = 0 \tag{2.4}$$

Thus the differential of moment is shear distribution. From beam theory,

$$M = EI\frac{d^2}{dr^2} \tag{2.5}$$

Also,

$$S = \frac{dM}{dr} = \frac{d}{dr}EI\frac{d^2w}{dr^2} \tag{2.6}$$

Hence we get the PDE for the beam bending as follows.

$$\boxed{\frac{\delta^2}{\delta r^2}\left(EI\frac{\delta^2 w}{\delta r^2}\right) + m\frac{\delta^2 w}{\delta r^2} - \frac{\delta}{\delta r}\left(T\frac{\delta w}{\delta r}\right) = f_z(r,t)} \tag{2.7}$$

2.1.1 Boundary conditions

The governing equation, as in Eq. 2.7 is a fourth order PDE in space and needs 4 boundary conditions. They are as follows:

(a) Cantilevered or fixed end

$$w = 0; \qquad \frac{dw}{dr} = 0$$

(b) Free end

$$M = EI\frac{d^2w}{dr^2}; \qquad S = \frac{d}{dr}\left(EI\frac{d^2w}{dr^2}\right) = 0$$

Also, since the only interest of this internship is to get the natural frequencies (free vibrations), set $f_z(r,t) = 0$.

2.1.2 Initial conditions

The beam PDE is second order in time and hence needs 2 initial conditions:
at $t = 0$, $\frac{\delta w}{\delta t}$ and w are prescribed.

Prasad ADHV Sample Report

2.2 Weak form of the governing equation

The weak form of the governing PDE is obtained by applying the Galerkin method. An assumed deflection is considered as a function which must satisfy all boundary conditions of the governing PDE. Then this assumed deflection function is substituted in the differential equation to get the weak form of the governing PDE.
Note: In the following sections r is substituted as x, so as to make it easier later on for implementation in MATLAB code. In the appendix, the assumption can be found that r is along the x- axis.
The series solution is assumed as:

$$w_{app} = \sum_{i=1}^{N} Y_i(x) q_i(t) \tag{2.8}$$

After substituting this approximate solution in the governing PDE, error is obtained. The the error is minimized by integrating the weighted function over the complete domain. In general, the error term is given by:

$$\epsilon(x,t) = m\ddot{w}_{app} + \frac{\delta^2}{\delta x^2}(EI\frac{\delta^2 w_{app}}{\delta x^2}) - \frac{\delta}{\delta x}(T\frac{\delta w_{app}}{\delta x}) - f_z \tag{2.9}$$

substituting the value of w_{app} from Eq.2.8, the weak form is obtained

$$\boxed{\epsilon(x,t) = \sum_{i=1}^{N}[mY_i\ddot{q}_i + (EIY_i'')''q_i - (TY_i')'q_i - f_z]} \tag{2.10}$$

2.3 Numerical modeling and implementation

The weak form obtained in previous section is further discretized and matrix form of each term is obtained so as to make it easier to implement the governing equation in computer code and solve it for solution, which in this case is the natural frequencies of the rotating cantilever beam. The error obtained is integrated over the domain using weighing function Y_j as follows:

$$\int_0^L \epsilon(x,t) Y_j dx = 0 \qquad\qquad j = 1, 2, ...N \tag{2.11}$$

$$\sum_{i=1}^{N}\left\{(\int_0^L Y_i Y_j m(x)dx)\ddot{q}_i + \int_0^L Y_j(EI(x)Y_i'')''dx - (\int_0^L Y_j(T(x)Y_i')'dx)q_i - \int_0^L Y_j f_z(x,t)dx\right\} = 0 \tag{2.12}$$

The above equation can be written as

$$\sum_{i=1}^{N}[m_{ij}\ddot{q}_i + K_{ij}q_i] = Q_i \qquad\qquad j = 1, 2, ...N \tag{2.13}$$

where,

$$m_{ij} = \int_0^L m(x)Y_iY_j dx \tag{2.14}$$

$$K_{ij} = \int_0^L Yj(EI(x)Y_i'')''dx - \int_0^L Y_j(T(x)Yi')'dx \tag{2.15}$$

$$Q_i = \int_0^L Y_i f_z(x,t)dx \tag{2.16}$$

The matrix form is $M\ddot{q} + Kq = Q$ which is a set of coupled differential equations. For free vibrations, set $Q = 0$ and, assume harmonic motion $q(t) = qe^{i\omega t}$. After applying this, a general algebraic eigenvalue problem is obtained as follows:

$$\boxed{\omega^2 Mq = Kq} \tag{2.17}$$

Prasad ADHAV Sample Report

2.3.1 Shape functions

Assuming polynomial distribution of displacement $w(x)$ within the element to be a cubic polynomial with four coefficients as there are 4 boundary conditions for the elements. The displacement $w(x)$ is given as:

$$w(x,t) = H_1 q_1 + H_2 q_2 + H_3 q_3 + H_4 q_4 = \sum_{i=1}^{4} H_i q_i \tag{2.18}$$

where, H_1, H_2, H_3 and H_4 are known as Hermite's shape functions, they are also known as interpolation functions or basis functions. The functions H_1 and H_3 have unit value at a node, zero at the other node, and their first derivatives H_2 and H_4 are zero at both nodes, but they are opposite in sign. It is clear that shape functions H_1 and H_3 represent deflection w, and H_2 and H_4 deal with the deflection slope θ. The shape functions are illustrated in the figure 2.3

$$H_1 = 2\left(\frac{x}{l}\right)^3 - 3\left(\frac{x}{l}\right)^2 + 1 \tag{2.19}$$

$$H_2 = \left[\left(\frac{x}{l}\right)^3 - 2\left(\frac{x}{l}\right)^2 + \frac{x}{l}\right] l \tag{2.20}$$

$$H_3 = -2\left(\frac{x}{l}\right)^3 + 3\left(\frac{x}{l}\right)^2 \tag{2.21}$$

$$H_4 = \left[\left(\frac{x}{l}\right)^3 - \left(\frac{x}{l}\right)^2\right] l \tag{2.22}$$

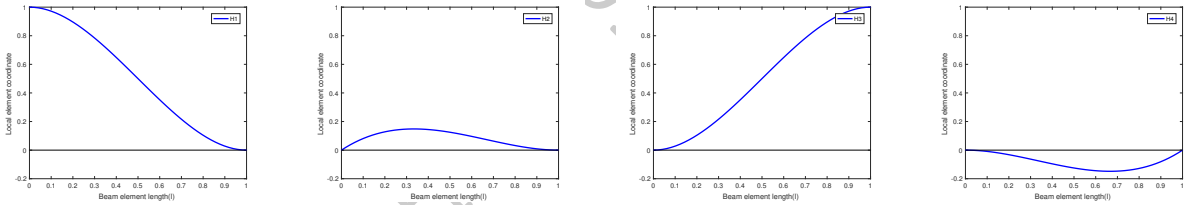

(a) H1 (b) H2 (c) H3 (d) H4

Fig 2.3 2-noded beam element Hermite's shape function

The above obtained displacement distribution polynomial is substituted as the Galerkin approximated solution as well as Galerkin weighing function in the discretized equation 2.12, and after applying integration by parts and simplifying the equations we get the following:

$$m_{ij} = \int_0^l m H_i H_j dx \tag{2.23}$$

$$K_{ij} = \int_0^l EI \frac{d^2 H_i}{dx^2} \frac{d^2 H_j}{dx^2} dx + \int_0^l T(x) \frac{dH_i}{dx} \frac{dH_j}{dx} dx \tag{2.24}$$

2.3.2 FEM matrices

Consider a beam element with uniform mass and stiffness properties. Assume that the left edge of an element is at a distance x_i from rotational axis and l is the element length as shown in figure 2.3. After solving the above equation for values of i and j, the following matrices are obtained. The degrees of freedom per node are 2, the degrees of freedom per element are 4, hence the elemental matrices

Prasad ADR Sample Report

obtained will be of sizes (4×4).
The mass matrix is given by:

$$m_{ij} = m \begin{bmatrix} \frac{13}{35}l & \frac{11}{210}l^2 & \frac{9}{70}l & \frac{-13}{420}l^2 \\ \frac{11}{210}l^2 & \frac{1}{105}l^3 & \frac{13}{420}l^2 & \frac{-1}{140}l^3 \\ \frac{9}{70}l & \frac{13}{420}l^2 & \frac{13}{35}l & \frac{-11}{210}l^2 \\ \frac{-13}{420}l^2 & \frac{-1}{140}l^3 & \frac{-11}{210}l^2 & \frac{1}{105}l^3 \end{bmatrix} \tag{2.25}$$

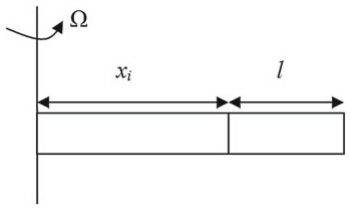

Fig 2.4 Element position on blade

The stiffness ,matrix is given as follows;

$$k_{ij} = EI \begin{bmatrix} \frac{12}{l^3} & \frac{6}{l^2} & \frac{-12}{l^3} & \frac{6}{l^2} \\ \frac{6}{l^2} & \frac{4}{l} & \frac{-6}{l^2} & \frac{2}{l} \\ \frac{-12}{l^3} & \frac{-6}{l^2} & \frac{12}{l^3} & \frac{-6}{l^2} \\ \frac{6}{l^2} & \frac{2}{l} & \frac{-6}{l^2} & \frac{4}{l} \end{bmatrix} + \frac{\omega^2 A_i}{2} \begin{bmatrix} \frac{6}{5l} & \frac{1}{10} & \frac{-6}{5l} & \frac{1}{10} \\ \frac{1}{10} & \frac{2l}{15} & \frac{-1}{10} & \frac{-l}{30} \\ \frac{-6}{5l} & \frac{-1}{10} & \frac{6}{5l} & \frac{-1}{10} \\ \frac{1}{10} & \frac{-l}{30} & \frac{-1}{10} & \frac{2l}{15} \end{bmatrix}$$

$$-m_i\omega^2 \begin{bmatrix} \frac{3}{5}x_i + \frac{6l}{35} & \frac{l}{10}x_i + \frac{l^2}{28} & \frac{-3}{5}x_i - \frac{6l}{35} & -\frac{l^2}{70} \\ \frac{l}{10}x_i + \frac{l^2}{28} & \frac{l^2}{30}x_i + \frac{l^3}{105} & \frac{-l}{10}x_i - \frac{l^2}{28} & \frac{-l^2}{60}x_i - \frac{l^3}{140} \\ \frac{-3}{5}x_i - \frac{6l}{35} & \frac{-l}{10}x_i - \frac{l^2}{28} & \frac{3}{5}x_i + \frac{6l}{35} & \frac{l^2}{70} \\ -\frac{l^2}{70} & \frac{-l^2}{60}x_i - \frac{l^3}{140} & \frac{l^2}{70} & \frac{l^2}{30}x_i + \frac{l^3}{105} \end{bmatrix}$$

where,

$$A_i = \sum_{j=i}^{N} (x_{j+1}^2 - x_j^2)$$

To understand the origin of term A, consider figure 2.4

Prasad ADHAV Sample Report

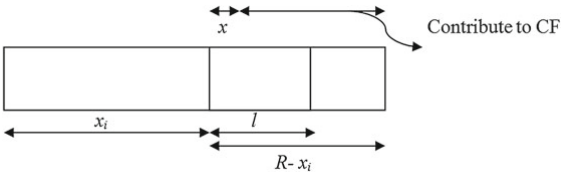

Fig 2.5 Contribution of centrifugal force

$$T(x) = \int_{x}^{L} m\Omega x dx = \int_{x_i}^{L} m\Omega^2 x dx - \int_{x_i}^{x_i+x} m\Omega^2 x dx$$

after solving the integration, the following equation is obtained

$$T(x) = \sum_{j=1}^{N} m_j \Omega^2 \frac{(x_{j+1}^2 - x_j^2)}{2} = \frac{\Omega^2 A_i}{2} - m_i \Omega^2 \frac{(x_i + x)^2 - x_i^2}{2} \tag{2.26}$$

2.3.3 Assembly of Elements

Suppose there is a beam which is divided into 4 equal size elements as shown in figure 2., the total strain energy is given as $U_{TOT} = U_1 + U_2 + U_3 + U_4$. Where, U_i is the strain energy for each element. The assembly in case of beam elements is fairly simple. As seen from the figure 2.5 2 nodes are common between any given two adjacent elements. The elements in the figure are shown within the element, in red. The size of the total stiffness matrix will be $2(n+1) \times 2(n+1)$, where n is the number of elements. In the following equations the elemental strain energies are shown, where symbols $+, \bigcirc, \times$ and $\square$ represent the matrix positions occupied by that element in the total stiffness matrix size matrix. It is clear that some positions in the different elements are overlapping, this is due to the shared nodes. These overlapping entries in the elemental stiffness matrices are late on simply added to each other in the assembly of stiffness matrices. The overlapping entries which are added are later denoted by $\oplus, \otimes$ and $\boxtimes$, simply representing the two different entry symbols added. The rest of the matrix, where there are no entries, those entries are nothing but zero.

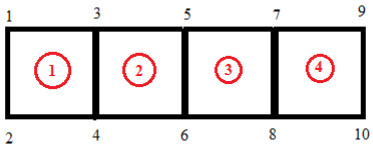

Fig 2.6 Meshed beam geometry

$$U_1 = \frac{1}{2}\begin{bmatrix} q_1 & q_2 & q_3 & q_4 & q_5 & q_6 & q_7 & q_8 & q_9 & q_{10} \end{bmatrix} \begin{bmatrix} + & + & + & + & & & & & & \\ + & + & + & + & & & & & & \\ + & + & + & + & & & & & & \\ + & + & + & + & & & & & & \\ & & & & & & & & & \\ & & & & & & & & & \\ & & & & & & & & & \\ & & & & & & & & & \\ & & & & & & & & & \\ & & & & & & & & & \end{bmatrix} \begin{bmatrix} q_1 \\ q_2 \\ q_3 \\ q_4 \\ q_5 \\ q_6 \\ q_7 \\ q_8 \\ q_9 \\ q_{10} \end{bmatrix}$$

Prasad 'DHAV Sample Report

$$U_2 = \frac{1}{2}\begin{bmatrix} q_1 & q_2 & q_3 & q_4 & q_5 & q_6 & q_7 & q_8 & q_9 & q_{10} \end{bmatrix} \begin{bmatrix} & & & & & & & & & \\ & & & & & & & & & \\ & & & & & & & & & \\ & & & & & & & & & \\ & & & & & & & & & \\ & & & & & & & & & \\ & & & & & & & & & \\ & & & & & & & & & \\ & & & & & & & & & \\ & & & & & & & & & \end{bmatrix} \begin{bmatrix} q_1 \\ q_2 \\ q_3 \\ q_4 \\ q_5 \\ q_6 \\ q_7 \\ q_8 \\ q_9 \\ q_{10} \end{bmatrix}$$

$$U_3 = \frac{1}{2}\begin{bmatrix} q_1 & q_2 & q_3 & q_4 & q_5 & q_6 & q_7 & q_8 & q_9 & q_{10} \end{bmatrix} \begin{bmatrix} & & & & & & & & & \\ & & & & & & & & & \\ & & & & & & & & & \\ & & & & & & & & & \\ & & & & \times & \times & \times & \times & & \\ & & & & \times & \times & \times & \times & & \\ & & & & \times & \times & \times & \times & & \\ & & & & \times & \times & \times & \times & & \\ & & & & & & & & & \\ & & & & & & & & & \end{bmatrix} \begin{bmatrix} q_1 \\ q_2 \\ q_3 \\ q_4 \\ q_5 \\ q_6 \\ q_7 \\ q_8 \\ q_9 \\ q_{10} \end{bmatrix}$$

$$U_4 = \frac{1}{2}\begin{bmatrix} q_1 & q_2 & q_3 & q_4 & q_5 & q_6 & q_7 & q_8 & q_9 & q_{10} \end{bmatrix} \begin{bmatrix} & & & & & & & & & \\ & & & & & & & & & \\ & & & & & & & & & \\ & & & & & & & & & \\ & & & & & & & & & \\ & & & & & & & & & \\ & & & & & & \square & \square & \square & \square \\ & & & & & & \square & \square & \square & \square \\ & & & & & & \square & \square & \square & \square \\ & & & & & & \square & \square & \square & \square \end{bmatrix} \begin{bmatrix} q_1 \\ q_2 \\ q_3 \\ q_4 \\ q_5 \\ q_6 \\ q_7 \\ q_8 \\ q_9 \\ q_{10} \end{bmatrix}$$

In the following equation, the assembled stiffness matrix is shown. As mentioned earlier, the assembly in case of these beam elements is simple addition, shown in the following equation.

$$K_{TOT} = K_{1234} + K_{3456} + K_{5678} + K_{78910}$$

$$K_{TOT} = \begin{bmatrix} + & + & + & + & & & & & & \\ + & + & + & + & & & & & & \\ + & + & \oplus & \oplus & \bigcirc & \bigcirc & & & & \\ + & + & \oplus & \oplus & \bigcirc & \bigcirc & & & & \\ & & \bigcirc & \bigcirc & \otimes & \otimes & \times & \times & & \\ & & \bigcirc & \bigcirc & \otimes & \otimes & \times & \times & & \\ & & & & \times & \times & \boxtimes & \boxtimes & \square & \square \\ & & & & \times & \times & \boxtimes & \boxtimes & \square & \square \\ & & & & & & \square & \square & \square & \square \\ & & & & & & \square & \square & \square & \square \end{bmatrix} \begin{bmatrix} q_1 \\ q_2 \\ q_3 \\ q_4 \\ q_5 \\ q_6 \\ q_7 \\ q_8 \\ q_9 \\ q_{10} \end{bmatrix}$$

Prasad ADHAV Sample Report

It should be noted that the mass matrix is assembled in similar way, as presented for stiffness matrix. In the boundary conditions section, it is defined that for fixed end, $w = \frac{dw}{dr} = 0$. Assuming that the fixed end for the beam considered here, to be on left end, q_1 and q_2 can be substituted as *zero*. Doing this, it is possible to eliminate the first *two* rows and first *two* columns of all the matrices in the equation.(For column matrix, only first *two* rows will be eliminated.)

2.3.4 Natural frequencies and Mode shapes

After obtaining the assembled matrices, the corresponding eigenvalue problem can be easily solved to obtain frequencies. Depending on the number of elements used, the corresponding number of first natural frequencies and their mode shapes can be obtained from the eigenvalues and eigenvectors respectively.

The i^{th} natural frequency of a beam can be found by using the i^{th} eigen value, denoted as λ_i. The following equation gives the natural frequency in rad/s.

$$\boxed{\omega_i = (\lambda_i L)^2 \sqrt{\frac{EI}{mL^4}}} \tag{2.27}$$

The mode shapes of the cantilever beam are obtained from the following equation:

$$\phi_i(x) = cosh(\lambda_i x) - cos(\lambda_i x) - \alpha_i(sinh(\lambda_i x) - sin(\lambda_i x)) \tag{2.28}$$

where,

$$\alpha_i = \frac{cosh(\lambda_i L) + cos(\lambda_i L)}{sinh(\lambda_i L) + sin(\lambda_i L)} \tag{2.29}$$

While obtaining the weak form of the governing equation for the rotating beam, for beam vibration problems, it is convenient to define displacement function in terms of mode shape functions, as follows:

$$w_{app} = \sum_{i=1}^{N} \phi_i(x) q_i(t) \tag{2.30}$$

The advantages of using mode shape function are that they satisfy all the boundary conditions fir the problem. Also, mode shape functions are orthogonal, hence the matrices are simple in structure.

2.3.5 Exact Natural frequency

The exact natural frequency for a non-rotating beam is available. It is easier to derive this frequency expression, since there are not complex partial derivatives involved. It is possible to obtain exact natural frequency expression, but the PDE involved is very complex, and the natural frequencies obtained from FEM are very close to these exact natural frequencies. The exact natural frequencies for rotating beam are obtained in a paper published by Wright et al. 1982.

$$\omega_i = (\lambda_j R)^2 \sqrt{\frac{EI}{mR^4}} \tag{2.31}$$

where, $\lambda_j R$ is given as follows, for i^{th} mode

i	1	2	3	4	j
$\lambda_j R$	1.8751	4.6941	7.8548	10.9955	$(2j-1)\frac{\pi}{2}$

Prasad ADHAV Sample Report

3 Results

A MATLAB code is implemented to solve the simple eigen value problem, derived in the last section. The code solves the eigenvalue problem, providing the user with eigenvalues and eigenvectors. These eigenvalues and eigenvectors are then used to find the natural frequency of a rotating beam. Four different cross-sections of beam are considered. Also, different rotational speeds are considered for obtaining the results. These frequencies are then validated using the published code from Ganguli 2017. The cases considered for study are explained in the following section.

3.1 Test Cases

A fairly common material used in low-pressure turbine is steel. The material properties considered for the steel are,Young's modulus $E = 2 \times 10^8$ n/m^2 and density $\rho = 8000$ kg/m^3. Four cross-sections are considered for the study, which are rectangle, square, circular and 4-digit NACA profile. They are shown in the figure 3.1. Furthermore, three 4-digit NACA profiles are considered, which are, NACA-0012, NACA-0015 and NACA-0018. The NACA profiles considered for study, all have closed trailing edge. The beam length for all the cross-sections considered is equal, which is $L = 1m$. The specifics of the cross-sections are illustrated in the figure 3.1

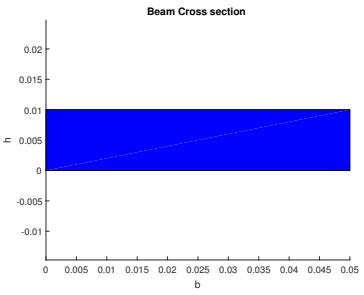

(a) Rectangle
$b = 0.05m \quad h = 0.01m$

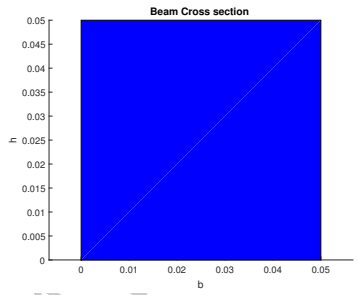

(b) Square
$b = 0.05m \quad h = 0.05m$

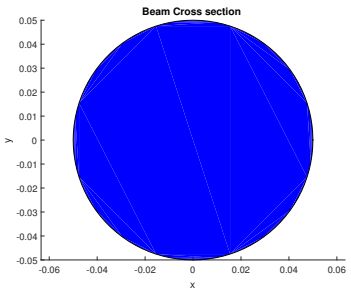

(c) Circle
radius $r = 0.05m$

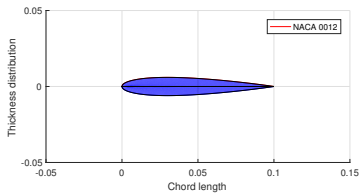

(d) NACA 0012
max thickness $= 0.12m$

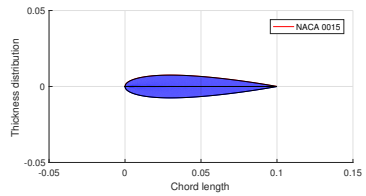

(e) NACA 0015
max thickness $= 0.15m$

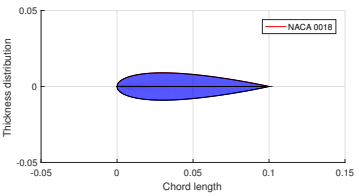

(f) NACA 0018
max thickness $= 0.18m$

Fig 3.1 Beam cross-sections considered for study

In the following figure, the 3 dimensional beam is represented for the different cross-sections. Also, please note, from NACA profiles considered, only figures for NACA 0012 will be used so as to avoid repetition and redundancy in the figures. Though, numerical results for all the profiles are presented in the following sections. Since the cross-section areas are different, it is expected that the frequencies obtained will vary from cross-section to cross-section.

Pre-DHA Sample Report

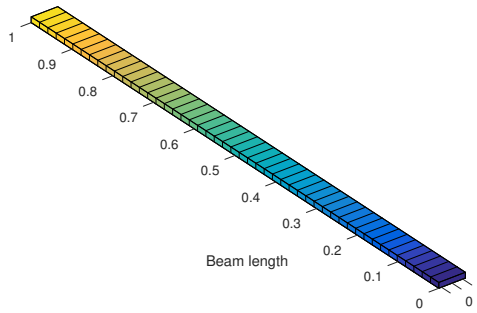

(a) Rectangular Beam

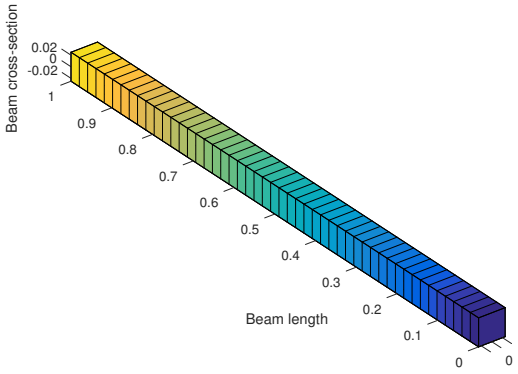

(b) Square Beam

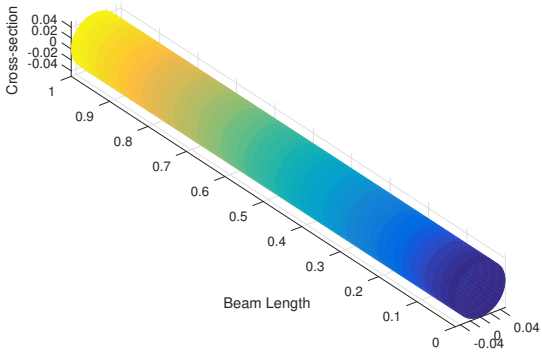

(c) Circular beam

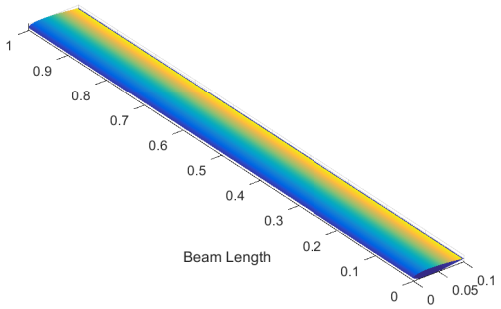

(d) NACA 0012 beam

Fig 3.2 3-dimensional beams

3.2 Natural Frequencies

For all the results obtained in this section, the number of elements used are 50 for all the beam cross-sections and all the rotating speeds considered. Only natural frequencies associated with first four modes are presented in the following section. This is because, when an impulse force is applied at the tip of the beam, almost all the modes are excited, but the most response contribution comes from first three or four modes. But since 50 elements are used in the MATLAB code, first hundred natural frequencies are obtained, which are presented in the appendix. The frequencies presented in all the sections have unit rad/s. For the study, for each cross-section, four rotational speeds are considered which are 0, 10, 25, 50, 157 and 377 rad/s. 157 rad/s(roughly $1500rpm$ is speed of helicopter rotor blades) and 377 rad/s(roughly $3600rpm$ is optimal opertaing speed of steam turbinein power generation.) These rotational speeds are considered since end goal is to find the natural frequencies of turbine blades discussed in the applications.

A log-log graph for each cross-section is presented, containing first 100 natural frequencies for the 4 rotating speeds considered for the study. Also, a log-log graph is presented containing first 100 natural frequencies for rotational speed of $10rad/s$, for all the cross-sections under consideration, so as to observe the co-relation.

Prasad ADHAV S

3.2.1 Rectangular beam

Rotating speed	mode 1	mode 2	mode 3	mode 4
0	1.6048	10.0573	28.1608	55.1840
10	5.11314	15.3547	34.0726	61.5660
25	11.9144	30.4364	54.8473	86.8759
50	23.3147	57.7322	96.1430	141.4750
157	72.1526	176.8630	282.1730	393.2690
377	172.6280	422.8030	669.8190	920.3960

Table 3.2.1 Natural frequencies of first 4 mode for rectangular beam and different rotating speeds

3.2.2 Square beam

Rotating speed	mode 1	mode 2	mode 3	mode 4
0	8.02417	50.2866	140.8040	275.9200
10	25.5657	76.7733	170.3630	307.8300
25	59.5721	152.1820	274.2360	434.3800
50	116.5740	288.6610	480.7150	707.3740
157	360.7630	884.3170	1410.8600	1966.3400
377	863.1390	2114.0100	3349.0900	4601.9800

Table 3.2.2 Natural frequencies of first 4 mode for square beam and different rotating speeds

3.2.3 Circular beam

Rotating speed	mode 1	mode 2	mode 3	mode 4
0	13.8983	87.0990	243.8800	477.9080
10	44.2811	132.9750	295.0770	533.1770
25	103.1820	263.5870	474.9920	752.3680
50	201.9110	499.9760	832.6230	1225.2100
157	624.8600	1531.6800	2443.6900	3405.8100
377	1495.0000	3661.5800	5800.8000	7970.8600

Table 3.2.3 Natural frequencies of first 4 mode for circular beam and different rotating speeds

3.2.4 NACA 0012 beam

Rotating speed	mode 1	mode 2	mode 3	mode 4
0	19.6985	123.4490	345.6600	677.3550
10	62.7612	188.4710	418.2240	755.6910
25	146.2430	373.5910	673.2220	1066.3600
50	286.1760	708.6340	1180.1100	1736.5300
157	885.63600	2170.9100	3463.5300	4827.1700
377	2118.9200	5189.6900	8221.6800	11297.4000

Table 3.2.4 Natural frequencies of first 4 mode for NACA 0012 beam and different rotating speeds

3.2.5 NACA 0015 beam

Rotating speed	mode 1	mode 2	mode 3	mode 4
0	22.0234	138.0180	386.4550	757.2980
10	70.1683	210.7140	467.5830	844.8780
25	163.5030	417.6830	752.6770	1192.2100
50	319.9510	792.2670	1319.380	1941.4800
157	990.1600	2427.1200	3872.3000	5396.8800
377	2368.9900	5802.1800	9192.0100	12630.7000

Prasad ADHAV Sample Report

Table 3.2.5 Natural frequencies of first 4 mode for NACA 0015 beam and different rotating speeds

3.2.6 NACA 0018 beam

Rotating speed	mode 1	mode 2	mode 3	mode 4
0	24.1254	151.1910	423.3400	829.5790
10	76.8656	230.8260	512.2120	925.5180
25	179.1090	457.5490	824.5170	1306.0000
50	350.4890	867.8860	1445.3100	2126.7800
157	1084.6700	2658.7800	4241.8900	5911.9900
377	2595.1100	6355.9800	10069.4000	13836.3000

Table 3.2.6 Natural frequencies of first 4 mode for NACA 0018 beam and different rotating speeds

It is clear from the tables presented above that due to the centrifugal stiffening effect,the natural frequency to achieve a particular mode increases with increase in the rotational speed. It is also observed that as higher modes are considered, the difference between frequencies required to achieve that mode reduces, with increase in rotational speed. It is also observed that for very high modes, there is minimum or almost no difference between frequencies for different rotational speed. Just this is illustrated with the log-log graph in figure 3.3. Though the graphs looks similar and in some cases identical, it is because the frequencies are close to each other, due to the close resemblance of the cross-sections to each other.

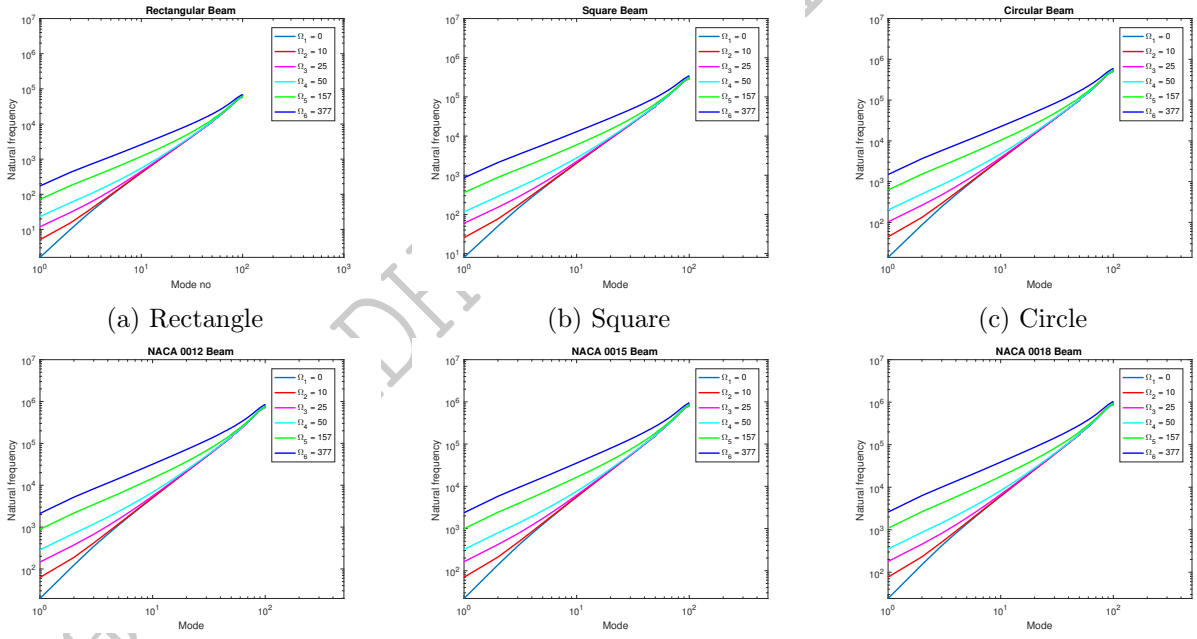

(a) Rectangle (b) Square (c) Circle

(d) NACA 0012 (e) NACA 0015 (f) NACA 0018

Fig 3.3 log-log graph of Natural frequencies v mode for all the rotational speeds under consideration

For lower rotating speeds, it is clearly observed that for any higher mode, the frequencies are almost same for different rotational speeds. Thus confirming the fact that centrifugal effect on natural frequency vanishes for higher modes. For higher rotating speeds it is observed that the natural frequencies are highly over-estimated. This error in solution can be traced to the shape function's inadequacy for capturing natural frequencies for higher rotating speeds.

Project Dissertation Report

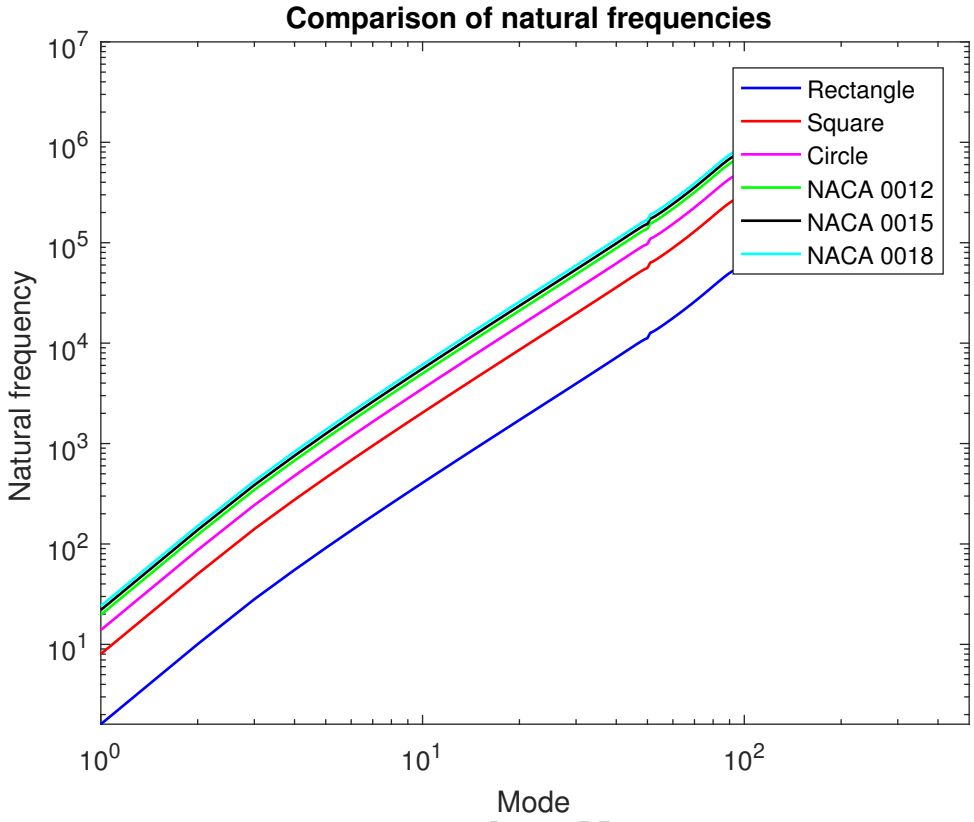

Fig 3.4 Natural frequencies for rotational speed of beam $\Omega = 0$

In the figure 3.4 the natural frequencies obtained at zero rotational speed for all the cross-sections are presented. In this graph, it is possible to easily observe the influence of corss-section on the natural frequency. Since the rectangular cross-sections has the least moment of inertia I_x, it is seen at the bottom, then followed by the square cross-section, circular beam, NACA 0012, NACA 0015 and finally NACA 0018. This is because the moment of inertia along x-axis is increasing, thus increasing the natural frequency of the beam. One more figure is presented below, showing the similar results as in figure 3.4, but for beam rotational speed $\Omega = 10 rad/s$. It is clearly observed that though the lines have shifted a little in positive y-direction (since there is increase in natural frequency with increase in rotational speed), but the ascending pattern of the cross-sections is the same.

Prasad ADHAV S

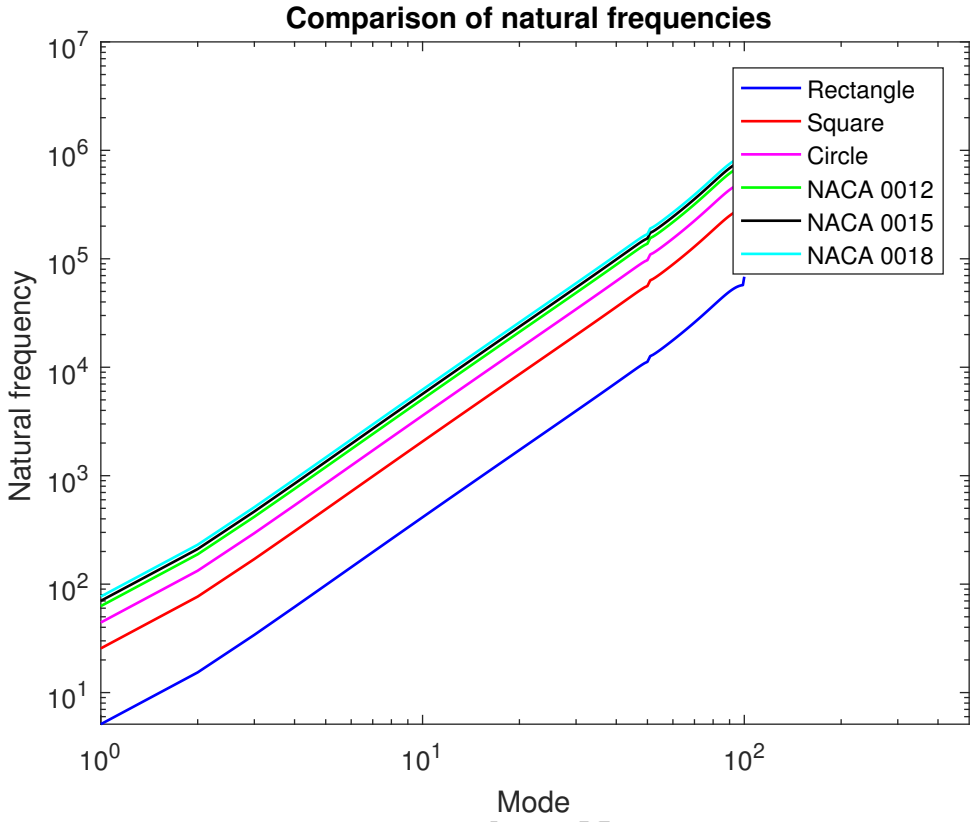

Fig 3.5 Natural frequencies for rotational speed of beam $\Omega = 10\ rad/s$

3.3 Mode Shapes

In this section, the first four mode shapes of the rotating cantilever beam are presented. The expression of mode shapes ϕ given in section 2.4.4 is implemented to produce the following plots. Both $2D$ and $3D$ plots are included. The mode shapes of square cross-section beam are presented as they best illustrates the mode shapes in the 3 dimensional view.

Prasad ADHAV S

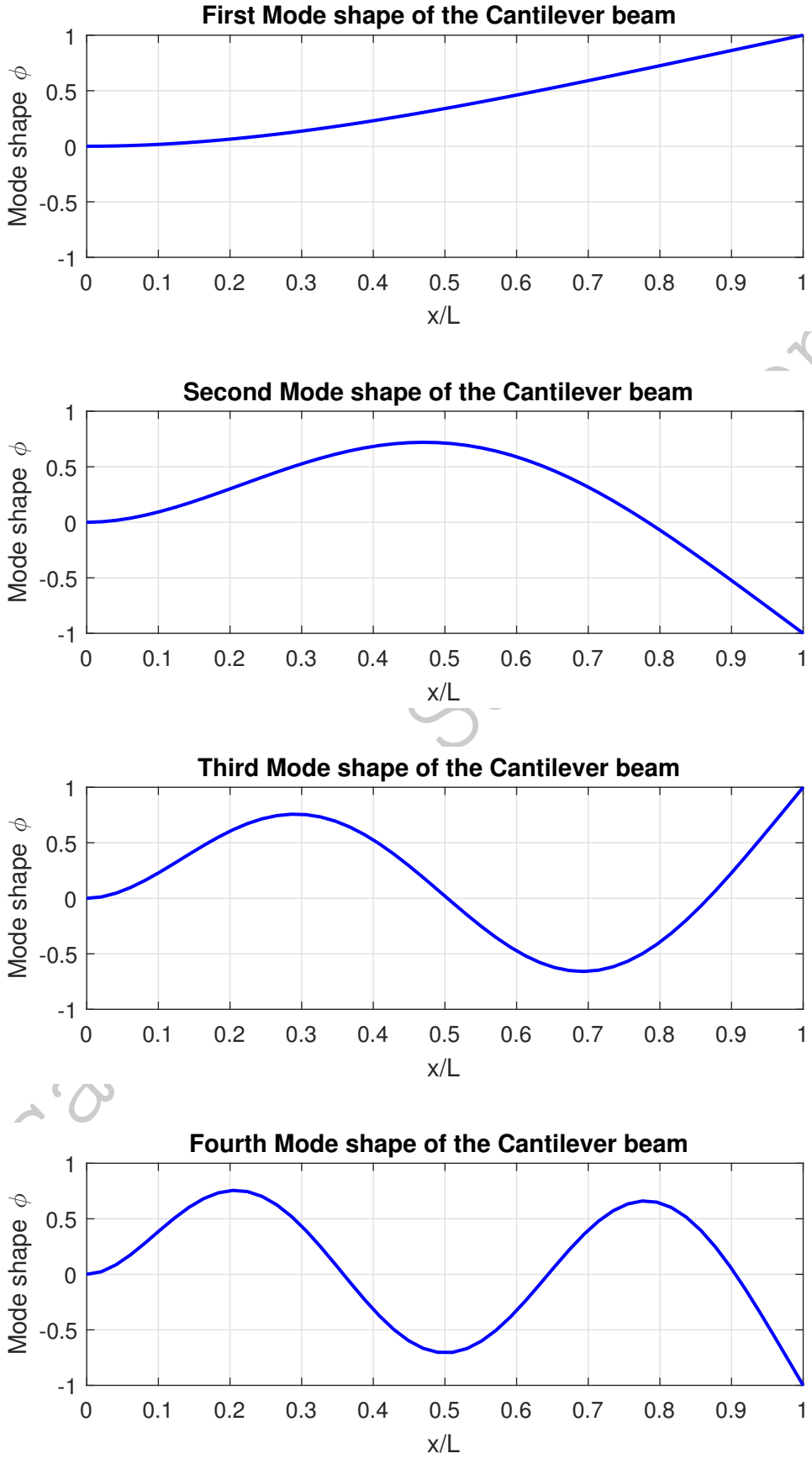

Fig 3.6 Modes shapes of square cantilever beam

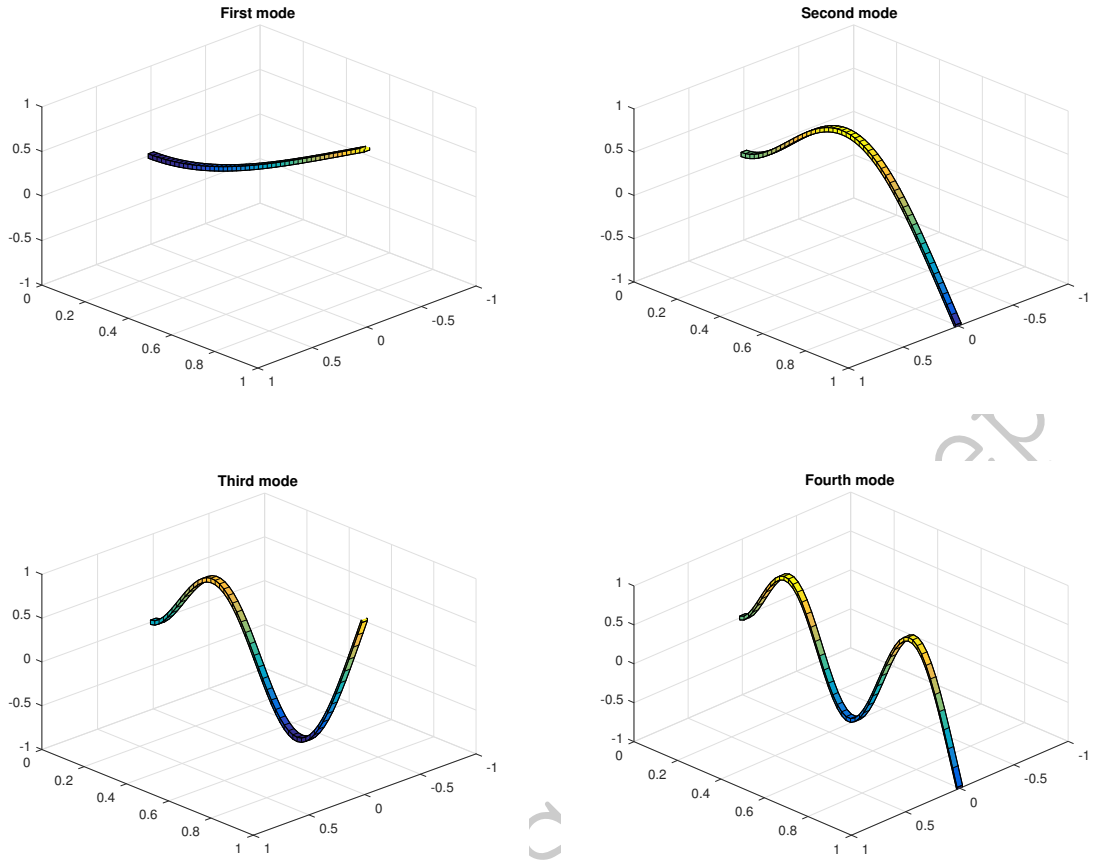

Fig 3.7 3D Modes shapes of square cantilever beam

3.4 Validation

The validation of the finite element method implemented for the rotating beam is done using pre-established Galerkin and Rayleigh-Ritz method. The MATLAB code for the same is provided in the appendix. The MATLAB code is very simple and requires few user inputs such as Young's modulus E, moment of inertia along x-axis I_x, mass per unit length m, length (radius) of the rotating beam R. Since, NACA profile are the utmost interest of the the study, NACA 0012 profile is used to validate the method presented in the earlier sections. The Galerkin and Rayleigh-Ritz provide natural frequencies only for non-rotating beams.

Method	mode 1	mode 2	mode 3	mode 4
Present method	19.6985	123.4490	345.6600	677.3550
Galerkin	19.733392	123.668063	346.276499	678.544361
Rayleigh	19.733478	123.667594	346.272678	678.526331

Table 3.4.1 Validation for first four mode natural frequencies for NACA 0012 non-rotating beam

In the following table, the numbers followed by name are the rotational speeds. The rotational speeds considered for validation are 10 and 25 rad/s.

Rotating speed	(in rad/s)	mode 1	mode 2	mode 3	mode 4
Present method	10	62.7612	188.4710	418.2240	755.6910
Ganguli	10	62.547237	188.259889	418.208569	755.414118
Present method	25	146.2430	373.5910	673.2220	1066.3600
Ganguli	25	146.215508	373.507055	673.214940	1066.344466

Table 3.4.2 Validation for first four mode natural frequencies for NACA 0012 rotating beam

Prasad ADHAV

From above tables it is clearly visible that the numerical implementation of the rotating beam is successful, as the frequencies are closely matched with the validation frequencies.
In post-process stage, the animations for the first four mode shapes are obtained, so as to illustrate the behavior of beam in each mode, and better understand the vibrations in a rotating cantilever beam.

3.5 Convergence study

In the convergence study it is seen how varying different parameters of the present method affect the accuracy of the solution obtained. In the following log-log graphs the percentile error for rotating as well as non-rotating beam are presented. The Galerkin exact solution is used for obtaining the error.

From the graphs the most apparent conclusion which can be drawn is that, by increasing number of elements(25 to 500), there is no significant change in the percentile error. The exception for this is when number of elements used are from 1 to 10, where the solution can be seen rapidly converging. In figure 3.8(a) it is also observed that the solution obtained for 2 elements is almost equal to the exact solution. This is a shear coincidence and nothing more. The present work uses 50 elements and results for the same are presented earlier, this is because for obtaining a good mode shape curve. Also, it was observed, there is no change or very insignificant change in natural frequencies for number of elements used 50. Hence, for minimum computations and optimum solution the present work uses 50 elements.

3.6 Future prospects

Apart from the structural design and analysis of a turbine blades, the ROM for rotating beam can be further improved and coupled with other systems, so as to get an almost real analysis. In the ROM of rotating beam the effects of hub radius can be included and the effect of the hub radius on the natural frequencies of rotor blades can be observed. In plane frequencies can be computed and the coupled effect of in-plane and out-of-plane frequencies on the rotor blade may be studied. This does complicates the problem a little but, the simulation is very close to real life problem. Furthermore, finite elements in fluid can be used to see the effects fluid forces on the rotor blades. Another option is to model the eigenvalue problem presented earlier, for non-linear geometries and non-linear material properties. For higher rotating speeds, a special shape function can be implemented which has capacity to capture natural frequencies at higher rotational speeds.
Since a turbine has multiple rotors, it is only natural to illustrate an example of And as shown in the following figure, multiple blades can be modeled so as to simulate a turbine. Three blades are considered with a square cross-section, since it is easier to perceive the deflections. A rotating speed of 10 rad/s is used and the first mode animation is simulated and 12 frames are captured to see the progressions of the beams. A hub radius of $0.1m$ is provided, which in this case is just a void. The hub is not plotted since it plays no role in the vibrational analysis and simulation considered here.

Prasad ADJAY Sample Report

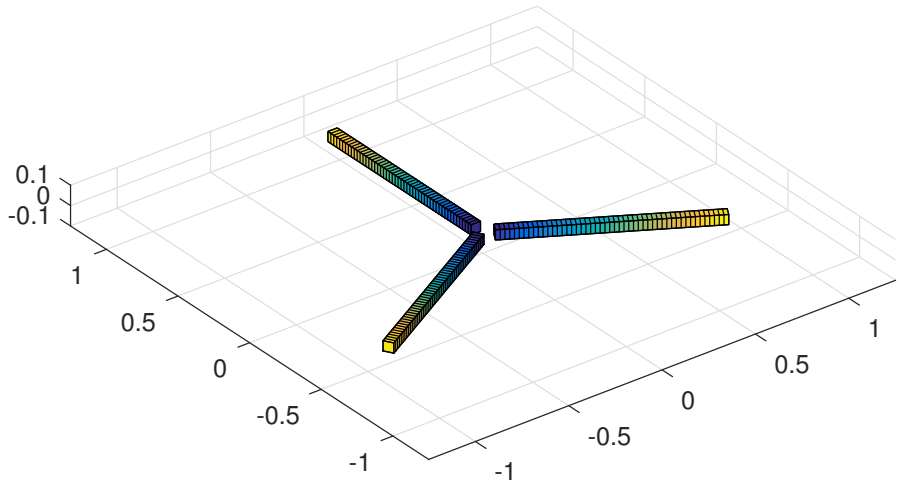

Fig 3.9 The multiple beams considered for the simulation

Prasad ADHAV Sa rt

4 Conclusions

A rotating beam model as a reduced order model for a rotor blade is successfully developed using the Timoshenko beam theory. The model is then numerically implemented in a MATLAB code, which solves the eigenvalue problem, and out of plane natural frequencies for rotating and non-rotating beam were obtained. For obtaining these natural frequencies, four different cross-sections are considered, rectangle, square, circle and 4 digit NACA profile. In the 4 digit NACA profile, 3 profiles are considered for the study, NACA 0012, NACA 0015 and NACA 0018. It is immediately visible that the cross-sections have increasing moment of inertia, the least is rectangle,then in ascending order, square, circle, NACA 0012, NACA 0015 and maximum NACA 0018. Though the last three don't have a significantly huge difference in their values. It is also observed that, moment of inertia has direct influence over the natural frequency of the beam. Hence, if we fix the rotating speed for all cross-sections, and consider any one of the first four modes, it can be observed that the natural frequency increases from rectangle to NACA 0018.

In the log-log graphs presented in figure 3.3 it can be seen that with increase in rotational speed the natural frequency for any particular mode increases. This is due to the centrifugal stiffening effect. The centrifugal force acting on the beam due to the rotation, actually makes it stiffer, thus increasing the natural frequency. This is very clearly observed for first few modes, but this centrifugal stiffening effect vanishes for higher modes as illustrated in figure 3.3. Also, it is apparent from the plots that centrifugal effect reduces with increase in rotating speed as well.

For validation the pre existing, well established Galerkin and Rayleigh-Ritz methods are utilized. These two methods are very simple, and are only implemented for non-rotating beams. Thus, the results obtained by setting $\Omega = 0$ are used. It is clear from the table 3.4.1 that the numerical implementation performed is correct. It is also seen that the frequencies obtained by these two methods are higher than the frequencies under examination. This is because Galerkin method over-estimates the solution and provides frequency values a little higher than the exact value. So it is safe to say that solution obtained is close to exact solution as well. The MATLAB code provided in Ganguli 2017, is used for the validation of the rotating beams. Hence two rotation speeds are considered for validation 10 and 25 rad/s. From table 3.4.2 it is clear that the model implemented is correct, for non-rotational as well as low rotational speeds. It is observed that for higher rotational speeds, the solution estimated is very high than it should be. This can be rectified by implementing some special shape functions. Due to the complex nature of these shape functions, they could not be implemented in short duration of time available for the internship.

A convergence study is presented for NACA 0012 beam. For few initial increments in the number of elements used, a rapid convergence is observed. As the number of elements goes on increasing no change or very insignificant change in percentile error can be observed. The percentile errors for non-rotating beams are very low, and it can be safely said the method implemented works correctly for non-rotating beam, as concluded from validation as well. But for rotating beams, when very few elements are used, the error in solution obtained is high. Hence it is advisable to use at least 25 elements for the present method.

The normalized mode shapes for the beam are plotted. But to see the behaviour of the beam, the vibrations of the beam are simulated. Also, multiple blades are simulated and there vibration in first mode is presented. First 12 frames of the animation are captured and present. It is seen that the beams are indeed vibrating out of phase. This is true for real life rotors in turbines.

The model developed can be further improved, and can have coupling effect of two or more variables. Such as Coriolis's effect, in-plane vibrations, hub radius effect. Furthermore this model can be coupled with a fluid model to give fluid effects on the rotor blade. By applying this very low computational power is required to solve the problem. And computationally as well as economically costly CFD tools won't be required, or at least can be avoided for the initial stages of design.

Prasad ADHAV Sample Report

References

[1] Stephen Timoshenko. *Strength of materials Part 1.* D. Van Nostrand Co., Inc, 1940.

[2] George Handelman, William Boyce, and Hirsh Cohen. *Vibrations of a uniform, rotating beam with tip mass.* United States Air Force, Office of Scientific Research, 1958.

[3] William E Boyce and George H Handelman. "Vibrations of rotating beams with tip mass". In: *Zeitschrift für angewandte Mathematik und Physik ZAMP* 12.5 (1961), pp. 369–392.

[4] Bruce E Goodwin. "On the realization of the eigenvalues of integral equations whose kernels are entire or meromorphic in the eigenvalue parameter". In: *SIAM Journal on Applied Mathematics* 14.1 (1966), pp. 65–85.

[5] Yudell L Luke. *Special functions and their approximations.* Vol. 2. Academic press, 1969.

[6] Louise H Jones. "The transverse vibration of a rotating beam with tip mass: the method of integral equations". In: *Quarterly of Applied Mathematics* 33.3 (1975), pp. 193–203.

[7] Dewey Yang Hodges and Michael Yang Rutkowski. "Free-vibration analysis of rotating beams by a variable-order finite-element method". In: *AIAA Journal* 19.11 (1981), pp. 1459–1466.

[8] AD Wright et al. "Vibration modes of centrifugally stiffened beams". In: *Journal of Applied Mechanics* 49.1 (1982), pp. 197–202.

[9] T Yokoyama. "Free vibration characteristics of rotating Timoshenko beams". In: *International Journal of Mechanical Sciences* 30.10 (1988), pp. 743–755.

[10] Adnan Ibrahimbegović. "On finite element implementation of geometrically nonlinear Reissner's beam theory: three-dimensional curved beam elements". In: *Computer methods in applied mechanics and engineering* 122.1-2 (1995), pp. 11–26.

[11] I Sharf. "Nonlinear strain measures, shape functions and beam elements for dynamics of flexible beams". In: *Multibody System Dynamics* 3.2 (1999), pp. 189–205.

[12] JR Banerjee. "Dynamic stiffness formulation and free vibration analysis of centrifugally stiffened Timoshenko beams". In: *Journal of Sound and Vibration* 247.1 (2001), pp. 97–115.

[13] David J Lucia, Philip S Beran, and Walter A Silva. "Reduced-order modeling: new approaches for computational physics". In: *Progress in Aerospace Sciences* 40.1-2 (2004), pp. 51–117.

[14] Gang Wang and Norman M Wereley. "Free vibration analysis of rotating blades with uniform tapers". In: *AIAA journal* 42.12 (2004), pp. 2429–2437.

[15] Jagadish Babu Gunda, Anuj Pratap Singh, et al. "Free vibration analysis of rotating tapered blades using Fourier-p superelement". In: *Structural Engineering and Mechanics* 27.2 (2007), pp. 243–258.

[16] Tan Bui-Thanh, Karen Willcox, and Omar Ghattas. "Model reduction for large-scale systems with high-dimensional parametric input space". In: *SIAM Journal on Scientific Computing* 30.6 (2008), pp. 3270–3288.

[17] Jagadish Babu Gunda and Ranjan Ganguli. "New rational interpolation functions for finite element analysis of rotating beams". In: *International Journal of Mechanical Sciences* 50.3 (2008), pp. 578–588.

[18] Wilhelmus HA Schilders, Henk A Van der Vorst, and Joost Rommes. *Model order reduction: theory, research aspects and applications.* Vol. 13. Springer, 2008.

[19] Chih Ling Huang, Wen Yi Lin, and Kuo Mo Hsiao. "Free vibration analysis of rotating Euler beams at high angular velocity". In: *Computers & structures* 88.17-18 (2010), pp. 991–1001.

[20] Kenneth Diest. *Numerical methods for metamaterial design.* Springer, 2013.

[21] E Onate. "Structural Analysis with the Finite Element Method, Vol. 2: Beams, Plates and Shells". In: *International Center for Numerical Methods in Engineering, Barcelona* (2013).

Prasad ADHAV Sample Report

[22] Ahmed A Shabana. *Dynamics of multibody systems*. Cambridge university press, 2013.

[23] Ranjan Ganguli. *Finite Element Analysis of Rotating Beams*. Springer, 2017.

[24] M Rafiee, F Nitzsche, and M Labrosse. "Dynamics, vibration and control of rotating composite beams and blades: A critical review". In: *Thin-Walled Structures* 119 (2017), pp. 795–819.

[25] Xiao-Dong Yang et al. "On the gyroscopic and centrifugal effects in the free vibration of rotating beams". In: *Journal of Vibration and Control* (2018), p. 1077546318774246.

Prasad ADHAV Sample Report

A Governing equation for rotating Timoshenko beam

Consider a Timoshenko beam element as shown in figure $C1$. The origin of this element is at a distance of r_i from the axis of rotation. The x-axis coincides with the centroidal axis of the beam. The y-axis is perpendicular and points away from the plane of paper. The z-axis is parallel to the axis of rotation and coincides with the axis of rotation of the beam. The uniform strain $\varepsilon(x)$ of the cross-section due to the centrifugal force $T(x)$ is given by,

$$\varepsilon(x) = \frac{T(x)}{EA} \tag{A.1}$$

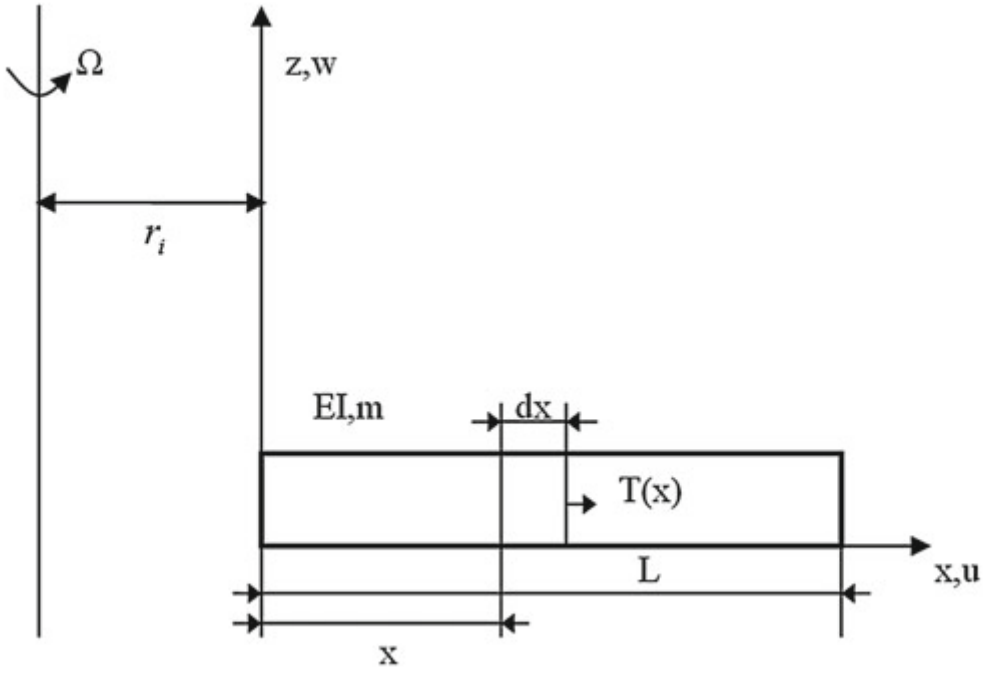

Fig C.1 Rotating Beam

Here, x is the distance of the cross-section from the origin. Also,

$$T(x) = \int_x^L \rho A \Omega^2 (r_i + x) dx = \left\{ r_i(L - x) + \frac{(L^2 - x^2)}{2} \right\} \tag{A.2}$$

The strain $\varepsilon_0(x)$ can be related to the axial displacement $u_0(x)$ by,

$$u_0'(x) = \varepsilon_0(x) = \frac{T(x)}{EA} \tag{A.3}$$

In Timoshenko beam theory, shear strain γ is given as,

$$\gamma = w' - \theta \tag{A.4}$$

where $w(x)$ is the flexural displacement of the beam neutral axis. The element dy deforms due to the combined axial and flexural displacements. At the left edge of the element, a point at a distance of $\bar{\eta}$ away from the neutral axis in the z-direction has the co-ordinates: $\{(x + u_0 - \bar{\eta}\theta), 0, (\eta \mp w)\}$. At the right edge, the corresponding point has the coordinates:

Prasad's Report

$$\left[\left\{x - u_0 - \bar{\eta}\theta + (1 + u_0' - \bar{\eta}\theta')dx\right\}, 0, (\bar{\eta} + w + w'dx)\right]$$

So, the strain of the element at a distance $\bar{\eta}$ from the neutral axis is,

$$\varepsilon(x,n) = \left[(1 + u_0' - \bar{\eta}\theta')^2 + (w')^2\right] - 1 \cong u_0' - \bar{\eta}\theta' + \frac{(w')^2}{2} \tag{A.5}$$

The strain energy due to flexure can be written as

$$U_f = \int\int\int_v \frac{E\varepsilon^2}{2} dV = \frac{E}{2}\int_A\int_0^L \left\{u_0' - \bar{\eta}\theta' + \frac{(w')^2}{2}\right\}^2 dxdA \tag{A.6}$$

This can alose written as

$$U_f = \frac{EA}{2}\int_0^2 (u_0')^2 dx + \frac{EI}{2}\int_0^L (\theta')^2 dx + EA\int_0^L u_0'(w')^2 dx \tag{A.7}$$

Since $A = \int_A dA$ and $I = \int_A (\bar{\eta})^2 dA$

Using equations A.2 and A.3, Eq. A.7 can be written as

$$U_f = C_1 + \frac{1}{2}\left[\int_0^L EI(\theta')^2 dx + \int_0^L T(w')^2 dx\right] \tag{A.8}$$

where C_1 is a constant.
The strain energy due to shear is

$$U_s = \int\int\int_v \frac{G\gamma^2}{2} dV = \frac{1}{2}\int_A\int_0^L G\gamma^2 dAdx = \frac{1}{2}kAG\int_0^L \gamma^2 dx \tag{A.9}$$

substituting γ yields,

$$U_s == \frac{1}{2}\int_0^L kAG(w' - \theta)^2 dx \tag{A.10}$$

Now, the total strain energy of the beam is given by

$$U = U_f + U_s = \frac{1}{2}\left[\int_0^L \left\{EI(\theta')^2 + T(w')^2 + kAG(w' - \theta)^2\right\} dx\right] + C_1 \tag{A.11}$$

Next, kinetic energy of the Timoshenko beam is to be calculated. Consider point at a distance of $\bar{\eta}$ from the neutral axis. The velocities at this point along the x, y and z directions are

$$V_x = -\bar{\eta}\dot{\theta},\ V_y = -\omega(x + u_0 - \bar{\eta}\theta),\ V_z = \dot{w} \tag{A.12}$$

The kinetic energy of the rotating Timoshenko beam is

$$J = \frac{1}{2}\int_A\int_0^L (V_x^2 + V_y^2 + V_z^2)\rho dAdx \tag{A.13}$$

After substituting Eq. C.12 into Eq. C.13, and simplifying the integral, the following equation is obtained

$$J = C_2 + \frac{1}{2}\left[\int_0^L \rho I(\omega^2\theta^2 + \dot{\theta^2})dx + \int_0^L \rho A\dot{w}dx\right] \tag{A.14}$$

Prasad ADHAV Sample Report

where C_2 is a constant. The Lagrangian L = J - U can now be written as,

$$L = \frac{1}{2}\int_0^L \{\rho I(\omega^2\theta^2 + \dot{\theta^2})\}dx - \frac{1}{2}\int_0^L \{EI(\theta')^2 + T(w')^2 + kAG(w' - \theta)^2\}dx + C_2 - C_1 \tag{A.15}$$

According to Hamilton's principle,

$$\delta \int_{f_1}^{f_2} Ldt = 0 \tag{A.16}$$

which leads to,

$$\int_{f_1}^{f_2}\int_0^L \{\rho I(\omega^2\theta\delta\theta + \dot{\theta}\delta\dot{\theta}) + \rho\dot{w}A\delta\dot{w}\}dxdt - \int_{f_1}^{f_2}\int_0^L \{EI\theta'\delta\theta' + Tw'\delta w' + kAG(w' - \theta)(\delta w' - \delta\theta)\}dxdt = 0 \tag{A.17}$$

Integrating by parts yields,

$$\int_{f_1}^{f_2}\int_0^L \{(Tw')' - \rho A\ddot{w} + kAG(w'' - \theta')\delta w dt\} + \int_{f_1}^{f_2}\int_0^L \{EI\theta'' + kAG(w' - \theta) - \rho I\ddot{\theta} + \rho I\omega^2\theta\}\delta\theta dt - \int_{f_1}^{f_2}[EI\theta'\delta\theta]_0^L dt$$

$$+ \int_{f_1}^{f_2}[-(Tw' + kAG(w' - \theta))\delta w]_0^L dt + \int_0^L [\rho I\dot{\theta}\delta\theta + \rho A\dot{w}\delta w]_{f_1}^{f_2} dx = 0 \tag{A.18}$$

Now, δw and $\delta\theta$ are completely arbitrary. The above equation therefore yields two equations, as

$$(Tw')' - \rho A\ddot{w} + kAG(w'' - \theta') = 0 \tag{A.19}$$

and the following equation obtained is the governing equation for rotating beam

$$\boxed{EI\theta'' + kAG(w' - \theta) - \rho I\ddot{\theta} + \rho I\omega^2\theta = 0} \tag{A.20}$$

The bending moment and shear force are also obtained as,

$$m = -EI\theta' \tag{A.21}$$

and

$$Q = -Tw' - kAG(w' - \theta) = -Tw' - M' - \rho I\ddot{\theta} + \rho I\omega^2\theta. \tag{A.22}$$

$K_{ij} = \int_0^l EI\frac{d^2H_i}{dx^2}\frac{d^2H_j}{dx^2}dx + \int_0^l T(x)\frac{dH_i}{dx}\frac{dH_j}{dx}dx$

Prasad ADHAV Sample Report

B 4 digit NACA Profile

The numbering system for 4 digit NACA profile is defined by: **NACA MPXX**.

where XX is the maximum thickness, t/c, in percent chord
M is maximum value of the mean line in hundredths of chord
P is the chordwise position of the maximum camber in tenths of the chord

Note that though the numbering system implies integer values, the equation can provide 4 digit foils for arbitrary values of M,P and XX. An example: NACA 2412 - a 12% thick foil, and a max value of the chamber line of 0.02, at $x/c = 0.4$. This profile can be seen in the figure $C.1$

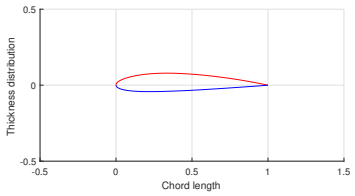

Fig $C.1$ The NACA 2412 profile example

The following MATLAB code $NACA.m$ illustrates the equation involved in obtaining the coordinates for any NACA profile. Here $y_t(x)$ is the thickness function and $y_c(x)$ is the chamber line function.

```
clc
clear all;
close all;
%% User Inputs
% Type of airfoil
  typeNACA = '0012';

% Extract values from type of airfoil string
Minit = str2double(typeNACA(1));
Pinit = str2double(typeNACA(2));
Tinit = str2double(typeNACA(3:4));

% Number of grid points
gridPts = 500;

% Constants
a0 = 0.2969;
a1 = -0.1260;
a2 = -0.3516;
a3 = 0.2843;
%a4 = -0.1015;     % Open trailing edge
a4 = -0.1036;      % Closed trailing edge

%% Calculations
% Actual percentage values of airfoil properties
M = Minit/100;
P = Pinit/10;
T = Tinit/100;
```

Prasad ADHAV Sample Report

```
% Airfoil grid
x = linspace(0,1,gridPts)';
z = linspace(0,1,gridPts);
zz = meshgrid(z,z);
% Camber and Gradient
yc     = ones(gridPts,1);
dyc_dx = ones(gridPts,1);
theta  = ones(gridPts,1);
for i = 1:1:gridPts
    if (x(i) >= 0 && x(i) < P)
        yc(i)     = (M/P^2)*((2*P*x(i))-x(i)^2);
        dyc_dx(i) = ((2*M)/(P^2))*(P-x(i));
    elseif (x(i) >=P && x(i) <=1)
        yc(i)     = (M/(1-P)^2)*(1-(2*P)+(2*P*x(i))-(x(i)^2));
        dyc_dx(i) = ((2*M)/((1-P)^2))*(P-x(i));
    end
    theta(i) = atan(dyc_dx(i));
end
% Thickness distribution
yt = 5*T.*((a0.*sqrt(x)) + (a1.*x) + (a2.*x.^2) + (a3.*x.^3) + (a4.*x
    .^4));

% Upper surface points
xu = x(:) - yt(:).*sin(theta);
yu = yc(:) + yt(:).*cos(theta);
% Lower surface points
xl = x(:) + yt(:).*sin(theta);
yl = yc(:) - yt(:).*cos(theta);

% Plot the airfoil (with lines)
figure(1);
hold on; grid on; axis equal;
plot(xu,yu,'r-'); patch(xu,yu,'b-');
plot(xl,yl,'b-'); patch(xl,yl,'b-');
xlim([-0.5 1.5]);  ylim([-0.5 0.5]);
xlabel('Chord length'); ylabel('Thickness distribution');

[XU,~] = meshgrid(xu,z);
YU = meshgrid(yu);
[XL,ZZ] = meshgrid(xu,z);
YL = meshgrid(yl);
c = ZZ;
figure(2)
s = surf(XU,ZZ,YU,c); s.EdgeColor = 'none';
hold on
s = surf(XL,ZZ,YL); s.EdgeColor = 'none';
hold off
grid on; axis image;
xlabel('Chord Length');zlabel('Thickness distribution');ylabel('Beam
   Length');
```

Prasad ADHAV Sample Report

C Validation

The following MATLAB codes are taken from Ganguli 2017 book, titled *Finite Element Analysis of Rotating Beams*.

C.1 *Validation_Galerkin.m*

```
% Code for Galerkin method using Uniform cantilever beam function

clc;
clear all;
syms x R O;

m = 5;                      % mass per unit length of the beam in kg/m
R = 1;                      % Radius of the beam in m
E = 2e+08;                  % For steel
I = 1.0417e-07;
EI= E*I;                    % Flexural Rigidity of beam in N-mĹ2
O = 0;                      % speed of Rotating Beam in rad/sec
                            % 0, 10, 25, 50
lam = 1.8751/R;             % Using Standard Table value of lambda for 1
    st mode
% lam = 4.6941/R;           % Mode 2
% lam = 7.8548/R;           % Mode 3
% lam = 10.9955/R;          % Mode 4

a = 0.7341;                 % Corresponding alpha value for mode 1
% a = 1.0185;               % Corresponding alpha value for mode 2
% a = 0.9992;               % Corresponding alpha value for mode 3
% a = 1.0000;               % Corresponding alpha value for mode 4

T = (m*O^2)*((R^2)-(x^2))/2;
T1= diff(T,x);

Y = (cosh(lam*x)-cos(lam*x)-(a*(sinh(lam*x)-sin(lam*x)))); % Beam
    function
m1 = int((m*(Y^2)),x,0,R); % Mass

Y1 = diff(Y,x);
Y2 = diff(Y1,x);
Y3 = diff(Y2,x);
Y4 = diff(Y3,x);

K11=int((Y*diff(diff(EI*Y2))),x,0,R);
K12=int((Y*diff(T*Y1)),x,0,R);
K = K11-K12;
K1 = vpa(simplify(K),4);

omsq = (K1)/(m1);          % Frequency obtained by (omegaĹ2)= K1/m1
omega = vpa(sqrt(omsq),4);% Actual Frequency of the beam in rad/sec
```

Prasad ADHAV Sample Report

C.2 *Validation_RayleighRitz.m*

```
% Code for Rayleigh Ritz method using Uniform cantilever beam function

clc;
clear all;
syms x R O;

m = 5;                      % mass per unit length of the beam in kg/m
R = 1;                      % Radius of the beam in m
E = 2e+08;                  % For steel
I = 1.0417e-07;
EI= E*I;                    % Flexural Rigidity of beam in N-mĹ2
O = 0;                      % speed of Rotating Beam in rad/sec
                            % 0, 10, 25, 50
lam = 1.8751/R;             % Using Standard value of lambda for 1st mode
% lam = 4.6941/R;           % Mode 2
% lam = 7.8548/R;           % Mode 3
% lam = 10.9955/R;          % Mode 4

a = 0.7341;                 % Corresponding alpha value for mode 1
% a = 1.0185;               % Corresponding alpha value for mode 2
% a = 0.9992;               % Corresponding alpha value for mode 3
% a = 1.0000;               % Corresponding alpha value for mode 4

T = (m*O^2)*((R^2)-(x^2))/2;
T1= diff(T,x);

Y = (cosh(lam*x)-cos(lam*x)-(a*(sinh(lam*x)-sin(lam*x)))); % Beam
    function
m1 = int((m*(Y^2)),x,0,R); % Mass

Y1 = diff(Y,x);
Y2 = diff(Y1,x);
Yi = int((EI*(Y2^2)),x,0,R);
Yt = int((T*(Y1^2)),x,0,R);

K = Yi+Yt;
K1= vpa(simplify(K),4);

omsq = K1/(m1); % Frequency obtained by (omegaĹ2)= K1/m1
omega = vpa(sqrt(omsq),4)% Actual Frequency of the beam in rad/sec
```

Prasad ADHAV Sample Report